

# Accurate Evaluation of Active-Site Density (SD) and Turnover Frequency (TOF) of PGM-Free Metal–Nitrogen-Doped Carbon (MNC) Electrocatalysts using CO Cryo Adsorption

Fang Luo,<sup>†</sup> Chang Hyuck Choi,<sup>‡</sup> Mathias J.M. Primbs,<sup>†</sup> Wen Ju,<sup>†</sup> Shuang Li,<sup>||</sup> Nathaniel D. Leonard,<sup>†</sup> Arne Thomas,<sup>||</sup> Frédéric Jaouen,<sup>\*,§</sup> and Peter Strasser<sup>\*,||</sup>

<sup>†</sup>Department of Chemistry, The Electrochemical Energy, Catalysis and Material Science Laboratory, Chemical Engineering Division, Technical University Berlin, , Straße des 17. Juni 124, 10623 Berlin, Germany

<sup>‡</sup>School of Materials Science and Engineering, Gwangju Institute of Science and Technology, Gwangju 61005, Korea

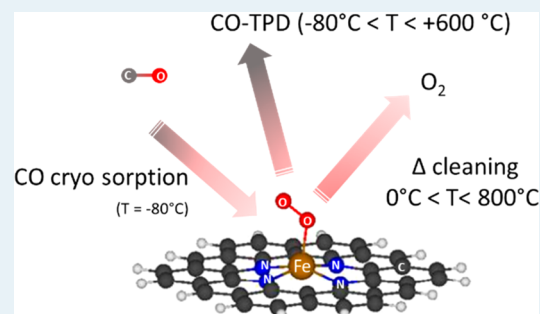
<sup>§</sup>Institut Charles Gerhardt Montpellier, UMR 5253, CNRS, Université de Montpellier, ENSCM, Place Eugène Bataillon, 34095 CEDEX 5 Montpellier, France

<sup>||</sup>Functional Materials, Department of Chemistry, Technical University Berlin, Hardenbergstr.40, 10623 Berlin, Germany

## Supporting Information

**ABSTRACT:** The number of catalytically active sites (site density, SD) and the catalytic turnover frequency (TOF) are critical for meaningful comparisons between catalytic materials and their rational improvement. SD and TOF numbers have remained elusive for PGM-free, metal/nitrogen-doped porous carbon electrocatalysts (MNC), in particular, FeNC materials that are now intensively investigated and widely utilized to catalyze the oxygen reduction reaction (ORR) in fuel cell cathodes. Here, we apply CO cryo sorption and desorption to evaluate SD and TOF numbers of a state-of-art FeNC ORR electrocatalyst with atomically dispersed coordinative FeN<sub>x</sub> (x ≤ 4) sites in acid and alkaline conditions. More specifically, we study the impact of thermal pretreatment conditions prior to assessing the number of sorption-active FeN<sub>x</sub> sites. We show that the pretreatment temperature sensitively affects the CO sorption uptake through a progressive thermal removal of airborne adsorbates, which, in turn, controls the resulting catalytic SD numbers. We correlate CO uptake with CO desorption and analyze the observed temperature-programmed desorption characteristics. The CO uptakes increased from 45 nmol·mg<sup>-1</sup><sub>catalyst</sub> at 300 °C cleaning to 65 nmol·mg<sup>-1</sup><sub>catalyst</sub> at 600 °C cleaning, where it leveled off. These values were converted into apparent SD values of 2.7 × 10<sup>19</sup> to 3.8 × 10<sup>19</sup> surface sites per gram catalyst. Because of similar ORR activity of the pristine catalyst and of the sample after 600 °C cleaning step, we conclude that the nature and number of surface FeN<sub>x</sub> sites remained largely unaffected up to 600 °C and that cleaning to less than 600 °C was insufficient to free the sites from previously adsorbed species, completely or partially impeding CO adsorption. Cleaning beyond that temperature, however, led to undesired chemical modifications of the FeN<sub>x</sub> moieties, resulting in higher TOF. In all, this study identifies and recommends a practical and useful protocol for the accurate evaluation of catalytic SD and TOF parameters of PGM-free ORR electrocatalyst, which enables a more rational future catalyst development and improvement.

**KEYWORDS:** PGM-free ORR electrocatalyst, site density (SD), catalytic turnover frequency (TOF), CO cryo sorption, CO cryo desorption, pretreatment temperature



## 1. INTRODUCTION

Carbon materials doped with atomically dispersed precious group metal (PGM)-free transition metal ions that are coordinated to up to four pyrrolic or pyridinic nitrogen atoms (forming a carbon-embedded molecular MN<sub>4</sub> moiety) are widely referred to as PGM-free MNC catalysts. They can be regarded, in the broadest sense, as solid-state analogues of molecular metal–porphyrin-type catalysts. Based on decades of previous work dealing with this family of solid catalysts, we know today that PGM-free MNC catalysts, in particular FeNC catalysts, hold the promise to replace precious metal catalysts

for the electrochemical reduction of molecular oxygen (ORR). The ORR is a key cathode reaction in fuel cells, metal–air batteries, and depolarized electrolyzers in the chlor–alkali industry.<sup>1–7</sup> Significant progress has been achieved in the design and catalytic performance PGM-free FeNC catalysts under the acidic conditions of proton-exchange membrane (PEM) fuel cells,<sup>7,8</sup> where they displayed an increasingly

Received: February 8, 2019

Revised: April 12, 2019

Published: April 15, 2019

competitive catalytic reactivity relative to state-of-the-art carbon-supported platinum, Pt/C, catalysts for the ORR.<sup>1,2,7,9</sup> FeNCs, however, are not competitive to Pt/C in terms of stability. Improvements in both directions require knowledge of type and number of the catalytic Fe-based active sites. However, the heterogeneity of the chemical state of Fe in many pyrolyzed FeNC catalysts (metallic or metal-carbide particles embedded in N-doped carbon, FeN<sub>x</sub> sites with diverse coordination and oxidation state of the metal) has typically rendered a clear identification of structure–property relationships difficult. The exclusive turnover frequency (TOF) of FeN<sub>x</sub> moieties has been particularly difficult to assess because of the lack of reliable methods to count and quantify the number of catalytically active FeN<sub>x</sub> moieties that are located on the top surface, the so-called active-site density (SD).

Several methods have been explored in the recent past years to probe active sites on pyrolyzed metal–NC catalysts and in some cases to estimate SD, including nitrite electrochemical stripping,<sup>10</sup> nitric oxide, tris(hydroxymethyl)aminomethane or cyanide as molecular probes,<sup>11–14</sup> or catechol as molecular probe for specific N-sites in N-doped carbon.<sup>15</sup> Carbon monoxide was early on proposed as a potential blocking adsorbate for the FeN<sub>x</sub> sites that catalyze ORR in MNC electrocatalysts.<sup>16–18</sup> However, in contrast to the known blocking effect of CO on the cytochromes that rely on the Fe-based heme active site, pyrolyzed FeNC catalysts were shown to remain essentially unaffected by the presence of CO when electrocatalyzing ORR at room temperature,<sup>16,19</sup> impeding the use of gaseous CO as a molecular probe for their FeN<sub>x</sub> active sites in such conditions.

Recently, it was reported that CO binds to individual FeN<sub>x</sub> sites of pyrolyzed FeNC materials if the adsorption temperature is lowered to about  $-80\text{ }^{\circ}\text{C}$  (Figure 1), allowing the

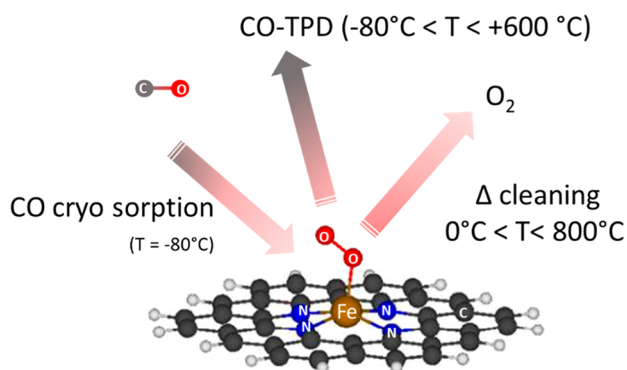


**Figure 1.** CO cryo adsorption and temperature-programmed desorption (TPD) enables counting of the catalytically active FeN<sub>x</sub> sites (shown here as slightly out-of-plane coordinative FeN<sub>4</sub> moiety) on the surface of precious group metal (PGM)-free Fe–N-doped porous carbon electrocatalysts (referred to generally as FeNC catalysts), provided the FeN<sub>x</sub> sites are freed up from previously bound adsorbates (here O<sub>2</sub> as an example) by a thermal cleaning prior to CO cryo sorption.

quantitative evaluation of gas-accessible adsorption sites.<sup>9,20</sup> The method involved consecutive CO pulse chemisorption at  $-80\text{ }^{\circ}\text{C}$ , followed by temperature-programmed CO desorption (TPD) during heating ramps to  $600\text{ }^{\circ}\text{C}$ . These sorption experiments were successfully applied as chemical interrogation tools to obtain quantitative insights into the mass-based density of CO-adsorbing sites in such catalysts, and a

positive correlation was established between this site density and the measured ORR activity.<sup>9,20</sup>

The ability of surface Fe-based sites to bind CO is however conditioned by their availability, implying either that no other adsorbates can be present on the surface FeN<sub>x</sub> moieties, or alternatively, that these adsorbates must be more weakly bonded than CO and thus can be spontaneously displaced during CO pulsing. With CO<sub>2</sub> and O<sub>2</sub> being likely adsorbates on FeN<sub>x</sub> sites exposed to ambient air, and considering that theory has predicted stronger binding of O<sub>2</sub> than CO on FeN<sub>x</sub> sites of FeNC catalysts,<sup>19</sup> measurable CO chemisorption on FeNC catalysts therefore requires a cleaning step prior to CO sorption, in order to remove any adsorbates, without chemical alteration of the catalyst material (see Figure 1). In our recent studies, the MNC catalysts were therefore cleaned prior to CO sorption by applying thermal annealing at  $600\text{ }^{\circ}\text{C}$ . However, no systematic study has been performed to date yet on the actual effect of the thermal cleaning conditions on the CO uptake, its desorption behavior, and hence on the resulting SD values and derived turnover frequency (TOF).

This is why, here, we investigate the influence of the cleaning temperature applied to FeNC prior to CO pulse chemisorption and subsequent temperature-programmed desorption (TPD) spectroscopy, covering a temperature range from  $50$  to  $800\text{ }^{\circ}\text{C}$ . We discuss the effect of cleaning temperature on the electrochemical activity, on the CO desorption kinetics, on the resulting experimental surface SD, and the average TOF for the catalytic oxygen reduction reaction derived from SD values and voltammetric data.

The FeNC catalyst studied here has been extensively characterized in previous work using electrochemical methods and various ex situ and in situ spectroscopic methods, including ex situ <sup>57</sup>Fe Mössbauer spectroscopy, ex situ and in situ X-ray absorption spectroscopy.<sup>21,22</sup> It was shown to exclusively comprise atomically dispersed FeN<sub>4</sub> moieties as Fe species, but in two main different coordination environments, as evidenced by the presence of two doublet components D1 and D2 in its <sup>57</sup>Fe Mössbauer spectrum (see Figure 1b in ref 21). The component D1 is usually assigned in the literature to Fe(II)N<sub>4</sub> environment in low spin state, and D2 to a Fe(II)N<sub>4</sub> or Fe(III)N<sub>4</sub> environment in medium spin state.<sup>23,24</sup> The relative amount of D1 and D2 species in the studied catalyst is 58 and 42% (see in ref 21 the Table SI and catalyst labeled Fe<sub>0.5</sub>), typical for FeNC catalysts comprising only or mostly FeN<sub>x</sub> moieties.<sup>25,26</sup> This catalyst is therefore representative of the class of pyrolyzed FeNC materials comprising Fe only as FeN<sub>x</sub> moieties, and the detailed investigation of the cleaning conditions applied before CO adsorption reported here has important implications for the quantification and assessment of the CO binding energy on different surface sites for this class of materials.

## 2. EXPERIMENTAL METHODS

**2.1. Synthesis.** The synthesis of the precious-metal group (PGM)-free FeNC powder catalyst (labeled Fe<sub>0.5</sub>NC, the subscript standing for the nominal weight% of Fe in the catalyst precursor before pyrolysis) involved a solid-state planetary ball milling of three different precursors, without involving any solvent or liquid. A mass of 15.8 mg of Fe(II) acetate (Fe(II)Ac, Sigma-Aldrich, purity 99.95%), 200 mg of 1,10-phenanthroline (phen, Sigma-Aldrich), and 800 mg of ZIF-8, a Zn(II) zeolitic imidazolate framework (Basolite Z1200 from BASF) were mixed in a ZrO<sub>2</sub> jar (45 mL), filled

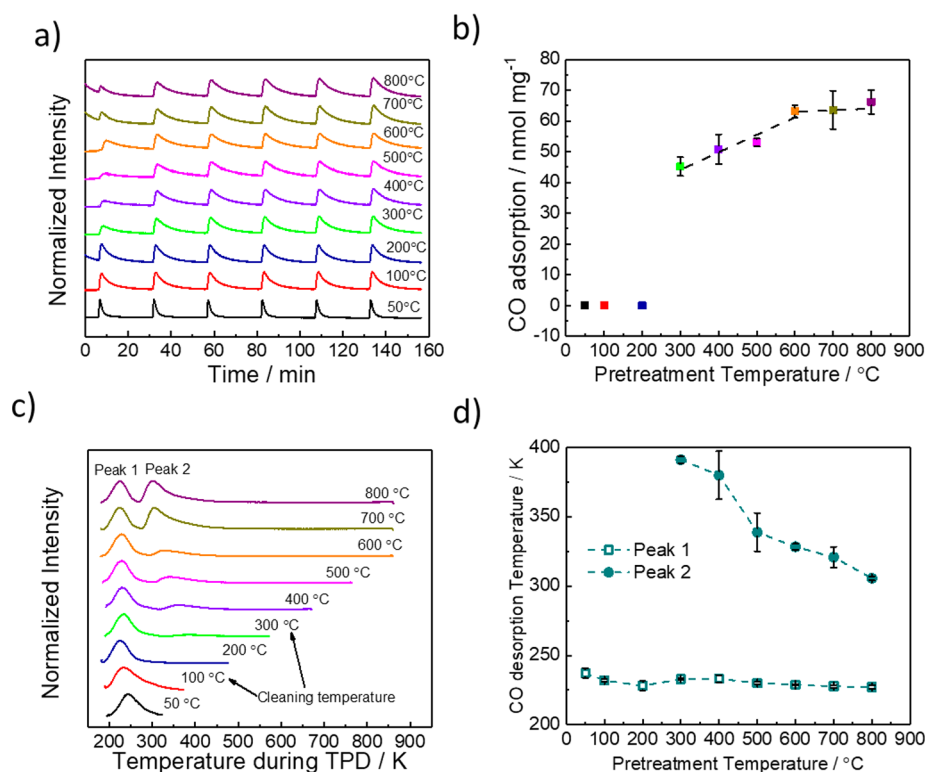


**Figure 2.** (a) CO pulse chemisorption at  $-80\text{ }^{\circ}\text{C}$  on the  $\text{Fe}_{0.5}\text{NC}$  catalyst after thermal annealing in He at the indicated temperature. (b) Mass-specific molar amount of CO adsorbed during the pulses at  $-80\text{ }^{\circ}\text{C}$  as a function of the annealing temperature. (c) Temperature-programmed desorption (TPD) profiles (labels denote annealing temperatures). (d) Desorption temperature peaks 1 and 2 vs annealing temperature. TPD was performed at a heating rate of  $10\text{ }^{\circ}\text{C min}^{-1}$ .

with 100 zirconium-oxide balls of 5 mm diameter, the jar sealed under air and placed in a planetary ball-miller (FRITSCH Pulverisette 7 Premium). Four cycles of 30 min of ball-milling are then performed, at a milling speed of 400 rpm, with a resting time of 5 min between each cycle. The resulting catalyst precursor is then collected, inserted in a quartz boat, itself installed in the middle of a quartz tube, and the tube purged with flowing Ar for 20 min. The oven is then heated to  $1050\text{ }^{\circ}\text{C}$  and equilibrated at that temperature for 90 min. After that equilibration time, the powder is directly introduced in the oven at  $1050^{\circ}$  under Ar flow via a heat-shock procedure, held at  $1050\text{ }^{\circ}\text{C}$  for 1 h, and the pyrolysis is stopped by opening the split hinge oven and removing the tube from the oven and letting it cool down under Ar flow. The resulting catalyst, denoted  $\text{Fe}_{0.5}\text{NC}$ , was collected after the tube cooled down and was not subjected to any acid-wash. It served as a reference catalyst throughout this work, and it was the precursor material for the annealing experiments described below.

**2.2. X-ray Photoemission Spectroscopy (XPS).** XPS was measured on K-Alpha + X-ray Photoelectron Spectrometer (XPS) System (Thermo Scientific), with Hemispheric  $180^{\circ}$  dual-focus analyzer with 128-channel detector. X-ray monochromator is microfocused Al  $K\alpha$  radiation. For the measurement, the as-prepared samples were directly pressed and loaded on the sample holder for measurement. The data was collected with X-ray spot size of  $400\text{ }\mu\text{m}$ , 20 scans for survey, and 50 scans for regions. For each sample, a survey and high-resolution C 1s, O 1s, N 1s, and Fe 2p regions were measured. The Avantage software with pseudo-Voigt Gaussian–Lorentzian product functions and Smart background was

used for peak deconvolution. Elemental concentrations were calculated from XPS peak area corrected by the corresponding sensitivity factors provided by the manufacturing company (SPECS).

**2.3. Annealing Conditions, CO Pulse Chemisorption, and Temperature-Programmed Desorption Spectroscopy (TPD).** All annealing, CO adsorption, and desorption experiments were conducted in a U-shaped quartz reactor inside a Thermo scientific TPD/R/O 1110 instrument (scheme see Figure S1) with TCD detector and combined mass spectrometer. In discussing CO uptake, SD, and TOF values, the pristine (as-synthesized)  $\text{Fe}_{0.5}\text{NC}$  material is labeled  $\text{Fe}_{0.5}\text{NC}$ . The  $\text{Fe}_{0.5}\text{NC}$  reference material was thermally pretreated by a single annealing step to  $600\text{ }^{\circ}\text{C}$  for 15 min in 20 sccm flowing helium prior to CO sorption measurement. The materials collected after the pristine (as-synthesized)  $\text{Fe}_{0.5}\text{NC}$  catalyst had been subjected to sequence of cleaning, CO uptake, and desorption cycles are labeled as “ $\text{Fe}_{0.5}\text{NC-T}$ ” where T is the maximum annealing temperature. More specifically, one single batch of the as-synthesized  $\text{Fe}_{0.5}\text{NC}$  powder catalyst underwent consecutive repeated cycles of (i) thermal annealing (pretreatment/cleaning) at  $50\text{ }^{\circ}\text{C}$  on the first cycle, then at  $100\text{ }^{\circ}\text{C}$  on the second cycle, at  $200\text{ }^{\circ}\text{C}$  on the third cycle, and so on up to a maximum temperature T of up to  $800\text{ }^{\circ}\text{C}$ ), (ii) CO pulse adsorption (CO uptake) at cryo conditions, and (iii) subsequent temperature-programmed CO desorption during reheating. The final upper temperature during the temperature-programmed desorption experiment was also set to be T, except for thermal pretreatments at  $700$  and  $800\text{ }^{\circ}\text{C}$ , where it was kept at  $600\text{ }^{\circ}\text{C}$  due to equipment constraints. The repeated (annealing-adsorption-desorption)

cycle experiment required 100–150 mg of the pristine Fe<sub>0.5</sub>NC catalyst powder.

The experimental details of each annealing (step 1) – adsorption (step 2) – desorption (step 3) cycle performed at the various temperatures was as follows: Step 1 involved heating the Fe<sub>0.5</sub>NC sample from room temperature to temperature T with a ramp rate of 10 °C min<sup>-1</sup> under continued 20 sccm 5N helium flow, followed by a hold of 15 min at T, and then followed by subsequent convective cooling back to room temperature. Step 2 involved subsequent cooling of the annealed catalyst to –80 °C, using a mixture of dry ice and acetone, followed by CO gas pulse chemisorption at –80 °C. Six consecutive 0.338 mL CO pulses, dosed at 25 min intervals, were passed through the catalyst samples, and the amount of CO retained in the catalyst was monitored and quantified using the TCD detector. Subsequently, in step 3, a temperature-programmed CO desorption (TPD) was performed by ramping the temperature from –80 °C up to the cleaning temperature T used during step 1, using a ramp rate of 10 °C min<sup>-1</sup> (same equipment and conditions used otherwise as for the CO pulses). Steps 1, 2, and 3 were repeated for each temperature up to the maximum temperature T, after which the powder was collected from the reactor. CO sorption data and all other physical and electrochemical characterizations of the catalysts labeled “Fe<sub>0.5</sub>NC-T” were conducted using the powders that had undergone these repeated annealing/CO sorption/CO desorption cycles.

**2.4. Electrochemical Measurements of ORR Activity and Selectivity.** Rotating-ring disk electrode (RRDE) studies were conducted using the pristine reference “Fe<sub>0.5</sub>NC” catalyst and both “Fe<sub>0.5</sub>NC-600” and “Fe<sub>0.5</sub>NC-800” catalysts. To prepare the catalyst ink, 15.7 mg of catalyst powder, 750 μL of deionized water, 190 μL of ethanol, and 60 μL of Nafion (5 wt % solution) were ultrasonicated for 15 min. The required aliquot of the ink was then drop cast on the glassy carbon disk (0.2475 cm<sup>2</sup>) to obtain a catalyst loading of 800 μg cm<sup>-2</sup>. A carbon rod and reversible hydrogen electrode (RHE) were used as counter and reference electrodes, respectively. The electrolyte was an O<sub>2</sub>-saturated aqueous solution of either 0.1 M KOH or 0.1 M HClO<sub>4</sub>. The disk potential range was scanned at 5 mV s<sup>-1</sup> from 0.05 to 1.1 V vs RHE in alkaline electrolyte and from 0.0 to 1.1 V vs RHE in acidic electrolyte. The potential for the ring was held at 1.2 V vs RHE. The collection efficiency of the RRDE electrode used was 0.37 ± 0.01.

**3. Results and Discussion.** PGM-free Fe<sub>0.5</sub>NC electrocatalysts with atomically dispersed FeN<sub>4</sub> moieties as the exclusive Fe species were prepared from metal organic framework precursors following previously reported synthetic procedures.<sup>2,7,21</sup> This particular catalyst has been repeatedly characterized in the past and constitute one of the most active family of PGM-free catalysts for the oxygen reduction reaction in acidic media.<sup>2,7,8</sup>

**3.1. Probing and Quantifying Surface Fe Sites with CO Ad/Desorption.** Figure 2 shows data from experiments addressing the effect of thermal annealing of the pristine PGM-free Fe<sub>0.5</sub>NC catalyst prior to CO chemisorption on the molar CO uptake during six consecutive CO pulses at cryo conditions of –80 °C. Figure 2c shows the subsequently monitored temperature-programmed desorption (TPD) profiles. We first discuss a control experiment in Figure S2 where we convinced ourselves that that no CO uptake occurred on Fe-free N-doped carbon (NC) catalysts even after a 600 °C

pretreatment (Figure S2 bottom CO pulse trace), suggesting that CO molecules adsorb exclusively on the atomically dispersed FeN<sub>x</sub> moieties on the surface of the FeNC material.

Figure 2a,b provides further evidence that there was no measurable CO adsorption on FeN<sub>x</sub> sites after thermal annealing at 50, 100, and 200 °C. Clearly, there was no CO uptake, either, on the nonannealed pristine Fe<sub>0.5</sub>NC material (not shown). CO uptake commenced between 200 and 300 °C and showed a molar value of 45 nmol CO/mg catalyst at 300 °C (Figure 2a,b). This is most plausibly explained by a competitive adsorption between CO and other FeN<sub>x</sub> site-blocking adsorbates that were preadsorbed on the pristine Fe<sub>0.5</sub>NC catalyst. Adsorbates may include water, atomic or molecular oxygen, molecular nitrogen, carbon dioxide, or trace amounts of airborne carbonous compounds always present under ambient catalyst storage and handling. With increasing annealing temperatures, the thermal cleaning of FeN<sub>x</sub> sites became more effective, and subsequent CO uptake increased linearly up to 600 °C, where it leveled off (Figure 2b). An obvious conclusion from this experiment in regards to an accurate determination of the number of surface FeN<sub>x</sub> sites is that the cleaning temperature quantitatively impacts the CO uptake and thus will sensitively impact the resulting SD analysis and the derived kinetic TOF value of a given non-PGM FeNC catalyst. The choice of a suitable thermal pretreatment conditions prior to CO uptake obviously requires care, in order to ensure an accurate site density value.

To learn more about the nature of the CO absorbing FeN<sub>x</sub> site, temperature-programmed CO desorption (TPD) spectroscopy was carried out after CO cryo chemisorption. To this end, the CO-loaded catalyst powder was slowly heated up to the temperature at which it was preannealed. This technique provides insight in desorption rates and CO sorption sites with distinct binding characteristics. As shown in Figure 2c, a low-temperature desorption peak (peak 1) was observed at all annealing (cleaning) temperatures and appears at a constant desorption temperature (Figure 2d squares). Starting at 300 °C, where CO began to adsorb (Figure 2b), a weak broad CO desorption peak near 380 K became discernible, referred to as TPD peak 2 (Figure S3, green curve). CO amounts based on integral areas of TPD peak 2 steadily grew with temperatures (Figure 2c and Figure S3). Control experiments evidenced that TPD peak 1 remained present after a thermal cleaning/cooling/heating protocol under He flow even in absence of CO pulsing and, in addition, even for Fe-free pure porous carbon samples. Coupled TPD-mass spectrometry (MS) experiments of Fe<sub>0.5</sub>NC and Fe/N-free pure porous carbon reference materials in presence and absence of CO pulsing evidenced beyond any doubt that the origin of peak 1 lied in the (physi)-desorption of trace levels of air from non-Fe sites, likely defects at graphene edges or in basal planes inside micro pores (Figure S4a and S4b). We note that 1 ppm of O<sub>2</sub> and 1 ppm of N<sub>2</sub> was quoted as being present in the commercial pressurized He cylinder used in the experiments. The accumulated amount of air over the experimentation time of several hours is sufficient to account for the observed peak 1 area.

The sudden emergence of CO uptake at 300 °C marked the initial availability of FeN<sub>x</sub> sites (referred to as “type 1” sites or site distribution) for CO chemisorption. We stress that this notation is not meant to relate to a single specific molecular structure, such as the D1- or D2-FeN<sub>x</sub> moieties identified by Mössbauer spectroscopy,<sup>2,7,8,21,24</sup> but is rather more generally

referring to a population of two or more FeN<sub>x</sub> sites with characteristic CO sorption and ORR catalytic activity. The mass-specific molar uptake of CO at 300 °C started at 45 nmol·mg<sup>-1</sup>. Between 400 and 600 °C, an ever larger ratio of type 1 FeN<sub>x</sub> adsorption sites became available due to increased adsorbate desorption rates with temperature (Figure 2b), while the CO TPD peak 2 shifted toward lower desorption temperatures, indicating enhanced CO desorption rates due to weaker CO surface binding (circles in Figure 2d). At and beyond 700 °C, the desorbed CO amount under TPD peak 2 increased sharply (Figure 2c and Figure S3), while the total CO uptake remained constant (Figure 2b). The plateau in the CO uptake evidence the complete, quantitative “cleaning” of all available surface FeN<sub>x</sub> sites.

During the annealing at 700 and 800 °C, we hypothesize that a partial, thermally induced chemical transformation of the type 1 FeN<sub>x</sub> site distribution into a somewhat different FeN<sub>x</sub> site distribution has occurred, here simply referred to as “type 2”. Again, the notation “type 2” is to imply a distinct distribution of 2 or more individual FeN<sub>x</sub> sites compared to the “type 1” distribution. Evidence for such a transformation is the sudden increase in the area of TPD peak 2 at constant overall CO uptake, suggesting the outgassing of additional species other than CO that must have formed during the high-temperature cleaning. We will provide evidence for this hypothesis in more detail below, where we also show that type 2 sites revealed a much larger intrinsic catalytic activity. After pretreatments at 700 and 800 °C, the desorption temperature of TPD peak 2 reached values as low as room temperature (Figure 2d), in agreement with earlier reports on other FeNC catalysts.<sup>9,20</sup>

The experimental trend between CO uptake (Figure 2b) and pretreatment temperature (50 to 800 °C) is the result of CO chemisorption on a population of FeN<sub>x</sub> adsorption sites that become increasingly available with temperature (up to 600 °C) before they start changing their chemical nature (above 600 °C). Type 1 FeN<sub>x</sub> sites required a minimum annealing temperature of 300 °C to become freed up from blocking adsorbates and be available for CO sorption. These “type 1” sites displayed a maximum total mass-based molar density of ca. 63 nmol mg<sup>-1</sup>. “Type 2” FeN<sub>x</sub> sites started evolving from type 1 FeN<sub>x</sub> sites beyond 600 °C, thereby keeping the total CO uptake constant. Both types of surface FeN<sub>x</sub> sites (if type 2 existed at all in the pristine Fe<sub>0.5</sub>NC catalyst) appeared to be blocked by air-borne, molecular adsorbates prior to thermal cleaning. Strong support for this derives from a control experiment, in which a Fe<sub>0.5</sub>NC catalyst, pretreated at 300 °C, exhibited reproducible CO uptake of 42–48 nmol/mg after pretreatment (Figure S5 bottom and center), however, showed no more CO uptake (0 nmol/mg) after pretreatment and immediate exposure to ambient air at room temperature (Figure S5 top). This demonstrates that adsorbates, most likely O<sub>2</sub> or CO<sub>2</sub>, did bind strongly enough on the FeN<sub>x</sub> surface sites to suppress subsequent CO sorption without renewed thermal cleaning.

The presence and emergence of a population of distinct types of FeN<sub>x</sub> sites on the surface is not unexpected, since previous structural characterization of pyrolyzed FeNC catalysts have indeed evidenced the existence of at least two dominant types of Fe sites. For example, <sup>57</sup>Fe Mössbauer spectroscopy has repeatedly shown two main doublets in all pyrolyzed FeNC catalysts, well-separated in their quadrupole splitting values, and assigned to atomically dispersed FeN<sub>x</sub>

moieties with different coordination geometry or different oxidation state and/or spin state of the central iron.<sup>21,24,27</sup> Also of interest, XPS studies on pyrolyzed FeNC catalysts have systematically revealed the coexistence of ferrous and ferric species, even for samples that only comprise FeN<sub>x</sub> sites and no metallic, oxide, or metal–carbide clusters.<sup>28</sup> Poisoning of FeN<sub>x</sub> centers with various probe molecules has also revealed the presence of two types of Fe-based sites on the surface, with different binding behaviors.<sup>12,14</sup> In particular, the hypothesis of the coexistence of ferrous and ferric FeN<sub>x</sub> moieties on the surface of pyrolyzed FeNC is appealing, since it would imply two separate levels of binding energy for any given adsorbate, and correlate with the CO-TPD observation. On a model system of a Fe-based MOF comprising both ferric and ferrous centers (MIL-100(Fe)), Wang et al. reported a similar observation to ours, that is, the cleaning of MIL-100(Fe) at 250 °C resulted in ca. twice higher amount of CO adsorbed subsequently, relative to the case after a cleaning step at only 50 °C.<sup>29</sup> The results were explained by the removal of preadsorbed water on a fraction of the Fe sites (coordinatively unsaturated sites) during the cleaning at 250 °C, resulting in the reduction of Fe(III) sites (when water is adsorbed) into Fe(II) sites. This implies that, after the 250 °C cleaning step, more Fe centers were in + II oxidation state (but in two different coordination environments) and able to then bind CO. While the material is obviously different, the concept may apply in our case as well, and one can postulate that the ferric and ferrous species observed on Fe<sub>0.5</sub>NC by XPS (see later) bind O<sub>2</sub> with different binding energies (stronger for the ferric species). The existence of divalent Fe species would imply two desorption events of preadsorbed O<sub>2</sub> or water and explain the complex dependence of CO uptake as a function of the cleaning temperature, as reported in Figure 2b. In parallel to those experimental works evidencing the presence of different FeN<sub>x</sub> sites, theoretical works have also considered different coordination geometries for FeN<sub>x</sub> moieties, which resulted in different binding energy for the O<sub>2</sub> adsorbate, for example. The DFT investigation of Zhang et al.<sup>19</sup> is of particular interest to the present study, showing that CO binding energy on FeN<sub>x</sub> can range from –1.35 to –3.78 eV for FeN<sub>4</sub>/C pyrrolic to FeN<sub>2</sub>/C on a zigzag edge (Table 3 in that work).

Finally, we turn to a more detailed discussion of the CO-TPD profiles of the samples annealed at 700 and 800 °C (dark yellow and purple curves in Figure 2c). As mentioned above, these profiles differ from the others in their significantly larger integral area of TPD peak 2 and in a marked decrease in the desorption temperature of peak 2 (Figure 2d). As discussed below in the electrochemistry section, the changes in the area of peak 2 appear closely linked to a sudden sharp increase in the catalytic ORR activity of the material; that is, they point to irreversible chemical changes in the material, possibly to thermally induced changes in the molecular Fe coordination, which is why we refer to them as a distinct type 2 Fe sites. We note that 700–800 °C is at the lower-limit of the temperature region typically used for pyrolytic synthesis and formation of ORR-active FeNC catalysts with active carbon-embedded FeN<sub>x</sub> sites, implying that reorganization of Fe, N, and C atoms became in principle possible at those temperatures. A plausible explanation for the sudden area increase of peak 2, indicating the desorption of additional adsorbates, is provided below with the discussion of the quantitative relation between ad-and desorption amounts.

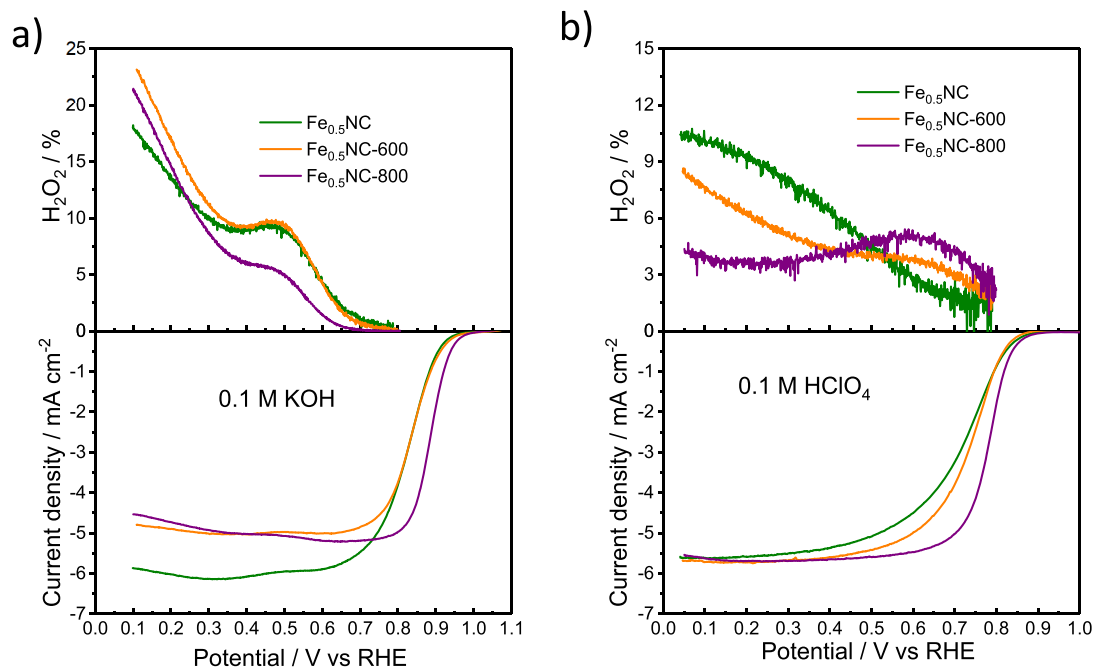


**Figure 3.** H<sub>2</sub>O<sub>2</sub> percentage and ORR disk current density from RRDE experiments of the reference Fe<sub>0.5</sub>NC, the Fe<sub>0.5</sub>NC-600 and the Fe<sub>0.5</sub>NC-800 catalysts at 1600 rpm in oxygen-saturated 0.1 M KOH (a) and 0.1 M HClO<sub>4</sub> (b). Temperature of 25 °C, geometric catalyst loadings of 0.8 mg cm<sup>-2</sup>, 5 mv s<sup>-1</sup> scan rate. Experimental errors of three independent measurements are reported in Table 1.

**3.2. Catalytic Oxygen Reduction (ORR) Activity and the Chemical State of the Catalyst Surface.** Figure 3 shows the measured RRDE sweep voltammograms representing the catalytic ORR reactivity in alkaline (Figure 3a) and acidic (Figure 3b) conditions of the Fe<sub>0.5</sub>NC reference catalyst, the Fe<sub>0.5</sub>NC-600, and Fe<sub>0.5</sub>NC-800 catalysts. The cumulative repeated thermal annealing cycles from 50 °C up to 600 °C prior to each CO ad/desorption of the Fe<sub>0.5</sub>NC-600 evidently did not have any effect on the experimental ORR activity nor chemical H<sub>2</sub>O<sub>2</sub> selectivity in the kinetic regime (disk current anodic of 0.8 V<sub>RHE</sub>, ring current anodic of 0.5 V<sub>RHE</sub>) compared to the Fe<sub>0.5</sub>NC reference catalyst (green and orange traces in Figure 2a,b). The only difference was the oxygen diffusion-limited disk current densities  $J_{lim}$ . The  $J_{lim}$  value of the reference Fe<sub>0.5</sub>NC was slightly above the theoretical value expected for a 4-electron ORR process. Assuming Levich's relation applies, this can be triggered by slightly higher roughness of the catalyst thin film layer, disturbing the laminar flow of the electrolyte above the catalyst layer on the rotating disk electrode at 1600 rpm rotation rate. The hydrogen peroxide selectivity in alkaline medium is identical within the experimental error for Fe<sub>0.5</sub>NC and Fe<sub>0.5</sub>NC-600.

The activity-selectivity performance of the Fe<sub>0.5</sub>NC-800 catalyst, however, differed sharply from the others in Figure 3a and b. The ORR activity after the cumulative thermal protocol up to 800 °C was markedly improved by a factor of around 5× and 3× in acidic and alkaline media, respectively. Table 1 provides detailed values of the kinetic current densities of each catalyst. Similarly, a simple Tafel slope analysis reveals a similar slope for Fe<sub>0.5</sub>NC, Fe<sub>0.5</sub>NC-600 and markedly different one for Fe<sub>0.5</sub>NC-800 (Figure S6) in alkaline and acidic electrolyte.

Considering that the experimental total CO uptake on FeN<sub>x</sub> sites of the Fe<sub>0.5</sub>NC-800 catalyst is, within the error, indistinguishable to those of the Fe<sub>0.5</sub>NC-700 or Fe<sub>0.5</sub>NC-600 catalysts (Figure 2b), we conclude that the higher kinetic

**Table 1.** Catalytic ORR Activities of Three Selected Catalysts in 0.1 M HClO<sub>4</sub> and 0.1 M KOH<sup>a</sup>

catalysts	0.1 M KOH (@0.9 V vs RHE)		0.1 M HClO <sub>4</sub> (@0.8 V vs RHE)	
	geometric current density (mA cm <sup>-2</sup> )	catalyst mass activity (mA mg <sup>-1</sup> )	geometric current density (mA cm <sup>-2</sup> )	catalyst mass activity (mA mg <sup>-1</sup> )
Fe <sub>0.5</sub> NC	0.43 ± 0.08	0.53 ± 0.10	0.89 ± 0.06	1.11 ± 0.08
Fe <sub>0.5</sub> NC-600	0.55 ± 0.10	0.67 ± 0.12	0.91 ± 0.05	1.14 ± 0.06
Fe <sub>0.5</sub> NC-800	2.36 ± 0.12	2.95 ± 0.15	2.28 ± 0.14	2.86 ± 0.18

<sup>a</sup>Reported are geometric current density and catalyst mass activity at 0.9 V<sub>RHE</sub> and 0.8 V<sub>RHE</sub> in 0.1 M KOH and 0.1 M HClO<sub>4</sub>, respectively.

ORR activity of the Fe<sub>0.5</sub>NC-800 catalyst must originate from an increased intrinsic catalytic ORR activity of the FeN<sub>x</sub> surface sites. As mentioned above, we believe that a thermally induced chemical modification of the FeN<sub>x</sub> sites of the Fe<sub>0.5</sub>NC-800 material plausibly explains the enhanced catalytic ORR activity. The discussion of the chemical state of the catalysts provided below will confirm this hypothesis. The CO-TPD peak 2 of Fe<sub>0.5</sub>NC-800 (purple curve in Figure S3) would be therefore related to CO desorption from chemically distinct FeN<sub>x</sub> sites compared to those present in the reference Fe<sub>0.5</sub>NC or those in all other Fe<sub>0.5</sub>NC-T (T between 50 and 600 °C) catalysts. The H<sub>2</sub>O<sub>2</sub> selectivity of Fe<sub>0.5</sub>NC-800 improved, as well, compared with that of Fe<sub>0.5</sub>NC and Fe<sub>0.5</sub>NC-600 (Figure 3a,b). This is plausible, as a kinetically favored 4-electron pathway invariably results in a lower peroxide yield.<sup>30</sup>

We now turn to the evolution of TPD peak 2 with pretreatment temperature (Figure 4a) as well as to a quantitative correlation between the area of CO uptake and CO TPD peak 2 in more detail. The area of TPD peak 2 increased in a nonlinear fashion with pretreatment temperature

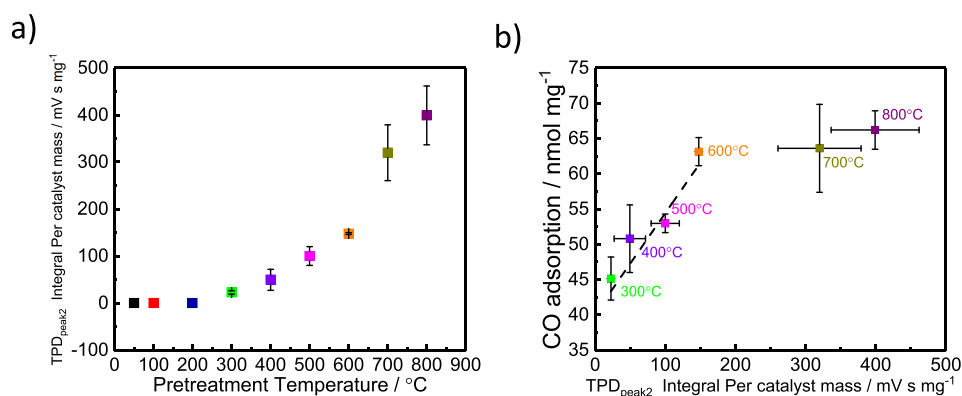


**Figure 4.** (a) TPD peak 2 integral area vs annealing temperature. (b) Correlation between the mass-normalized molar amount of CO adsorbed during pulse chemisorption and the mass normalized integral area of the high-temperature CO TPD peak 2. A linear fit is shown for the annealing temperatures 300–600 °C.

up to 600 °C, somewhat resembling a thermally activated process. Beyond 600 °C, a clearly sharper stepwise increase in peak area occurred. Given a similar CO uptake (Figure 2b), this could suggest the desorption of molecules other than CO. Then, we verified that there was a fairly linear correlation between CO chemisorption and CO desorption up to temperatures of 600 °C. A plot of the total molar CO uptake versus the integral area of TPD peak 2 indeed displayed a proportionality over this range (Figure 4b). This demonstrates that CO chemisorbed on the FeN<sub>x</sub> sites strongly enough for subsequent TPD detection. An absolute calibration of the CO TPD peak 2 areas, however, was not possible. This is why the *x*-axis in Figure 4 reports integral TPD peak areas rather than absolute molar CO amounts. The catalysts annealed up to 700 °C and up to 800 °C showed significantly larger integral areas of TPD peak 2 compared with those of TPD peak 1 (Figure 2c and Figure S3).

Given the possibility of thermally induced and residual oxygen-induced chemical and structural modifications of the catalysts during the annealing at 700 and 800 °C, we are inclined to ascribe the reduced uptake of residual air from the He stream (see smaller TPD peak 1 in Figure S3 and Figure 2) to chemical changes, likely carbon oxidation, in the catalyst microporous structure. This is plausible because residual molecular oxygen, even at the ppm level in the commercial 5N helium, becomes sufficiently reactive beyond 600 °C and leads to oxidation of carbon defects (graphene sheet edges or basal planes). Upon cooling the catalyst to –80 °C under continued flowing helium, less molecular oxygen was trapped in the catalyst porous structure and the smaller TPD peak 1 ensues (Figure 2c). During TPD heating (Figure 2c), the additional oxygenated surface groups on the carbon surface can desorb as CO<sub>2</sub> (see Figure S4a) along with the adsorbed CO adsorbates, adding high-temperature tailings in Figure S3. We believe that this combined desorption accounts at least partially for the larger TPD peak 2 areas.

To assess the effects of the thermal annealing and cleaning pretreatment on the molecular chemical structure of the pristine Fe<sub>0.5</sub>NC catalyst, a number of molecular characterization techniques are available, such as X-ray absorption, X-ray photoemission, or Mössbauer spectroscopy. However, since the focus of this work centered on CO cryo sorption/desorption and voltammetry to evaluate SD and TOF values, rather than on the analysis of the detailed molecular changes of the catalysts and their active sites with temperature, we

refrained from applying a wide array of analytical techniques but limited ourselves to low- and high-resolution X-ray photoemission spectroscopy (XPS) in the C 1s, O 1s, N 1s, and Fe 2p regions (Figure 5, Figure S7, and Figure S8) to study the chemical state and electronic environment of the atomic constituents (Table S1 and Table S2) of the Fe<sub>0.5</sub>NC reference catalyst, the Fe<sub>0.5</sub>NC-600 and Fe<sub>0.5</sub>NC-800 catalysts. Figure 5d shows the near-surface elemental concentrations obtained from a quantitative peak analysis of the C, N, O and Fe core level spectra. The elemental trends indicate the stepwise thermal removal of atomic nitrogen and atomic oxygen as adsorbates or from the lattice, with atomic oxygen likely stemming from O-blocked FeN<sub>x</sub> sites or oxygenated surface groups on nearby carbons. XPS results are in line with the notion that structural reorganization processes in the surface of the catalyst past 600 °C have led to a slight decrease in nitrogen content. The speciation of the narrow-scan spectra in the N 1s range of Fe<sub>0.5</sub>NC, Fe<sub>0.5</sub>NC-600 and Fe<sub>0.5</sub>NC-800 are presented in Figure 5e and were derived from Figure 5a–5c. The reference catalyst showed different types of N functionalities with range of binding energies (Figure 5a), as typically observed for pyrolyzed FeNC catalyst. The same N species are also present after the cleaning protocol up to 600 and 800 °C (Figure 5b,c). For a more detailed comparison, the N 1s spectra were fitted using five commonly considered nitrogenated components, and with positions in the order of increasing binding energy, component 1 with peak position fixed at around ~398.5 eV (pyridinic nitrogen), component 2 fixed at ~399.6 eV (N in metal–N<sub>x</sub> or C–NH<sub>2</sub> or quaternary),<sup>20,31–38</sup> component 3 fixed at ~401.2 eV (pyrrolic nitrogen), component 4 at ~402.4 eV (graphitic nitrogen), and component 5 fixed at ~403.7 eV, which was assigned to N-oxide. Changes in the relative concentration of N species in the three samples are shown in Figure 5e. There are no significant changes in relative concentrations of the different N species, except perhaps for a trend of increasing content of graphitic N in the order Fe<sub>0.5</sub>NC < Fe<sub>0.5</sub>NC-600 < Fe<sub>0.5</sub>NC-800. As to the chemical state of oxygen, Figure S7b suggested no significant changes in the O 1s core level spectra between Fe<sub>0.5</sub>NC, Fe<sub>0.5</sub>NC-600, and Fe<sub>0.5</sub>NC-800.

The relatively low signal-to-noise ratios of the Fe<sub>2p</sub> core level spectra in Figure S7c (Fe 2p<sub>3/2</sub> at 709.5–711 eV and Fe 2p<sub>1/2</sub> at 723–724 eV) were caused by the low absolute Fe contents of the three catalysts. Still, Figure S7c suggested some subtle changes in the Fe 2p<sub>3/2</sub> region of the Fe<sub>0.5</sub>NC-600 and

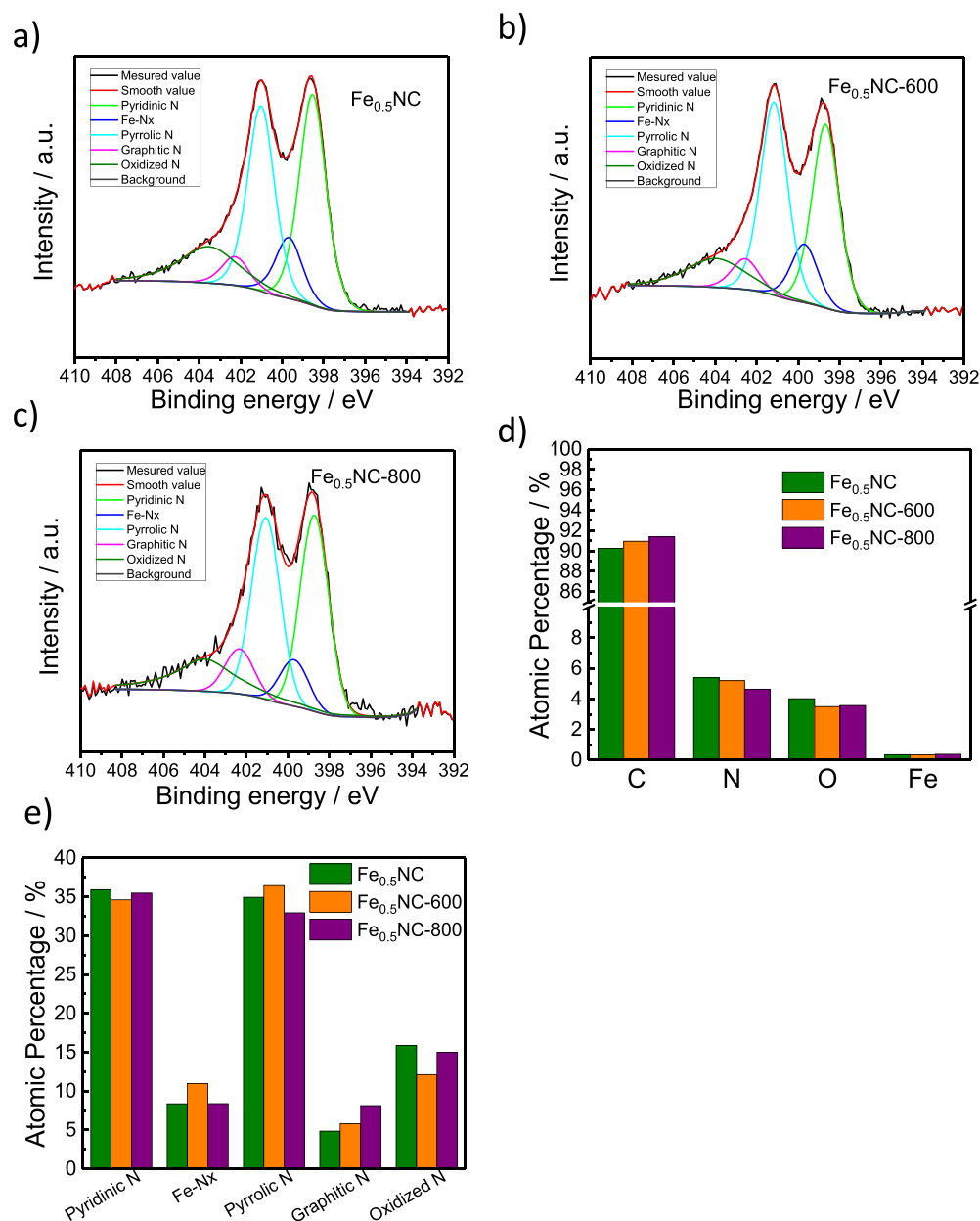


**Figure 5.** XPS comparative investigation of Fe<sub>0.5</sub>NC, Fe<sub>0.5</sub>NC-600, and Fe<sub>0.5</sub>NC-800. Narrow-scan spectra of N 1s and their fittings with different species (a,b,c). The bar plots show the atomic content of C, N, O, and Fe (d) and the relative content of different nitrogen groups (e).

Fe<sub>0.5</sub>NC-800 compared with the reference Fe<sub>0.5</sub>NC. A more detailed peak analysis (Figure S7d–f) combined with quantitative Fe speciation (Table S2) revealed that thermal treatment up to 600 °C resulted in a larger proportion of ferric Fe<sup>III</sup> (710.8–711.8 eV), possibly because of the prolonged exposure to oxygen trace amounts during He flow or caused by cleaning of more and more FeN<sub>x</sub> moieties followed by oxygen readorption and oxidation by oxygen from ambient air in the transfer to the X-ray photoemission analysis.

The fact that the experimental ORR reactivity in the kinetic region remained unaffected by the annealing at 600 °C demonstrates that the thermally induced Fe redox states changes were largely reversible and were ultimately determined by the voltammetric protocol. Annealing at 800 °C, in contrast, decreased the ferric Fe<sup>III</sup> content relative to the Fe<sub>0.5</sub>NC-600 in favor of ferrous Fe<sup>II</sup> (707.1–709.4 eV), which reflects the chemical reactivity and increasing reducing power of the

carbonous environment. These changes in the distribution of the chemical state of Fe after annealing at 800 °C (referred to as type 2 sites), while in themselves likely reversible, as well, were likely coupled with irreversible modifications in the geometric coordinative environment of the Fe central ion, accounting for the enhanced ORR reactivity. The presence of metallic Fe<sup>0</sup> (706.7–707.2 eV) and hence metallic Fe nanoparticles could be safely excluded in all three catalysts and under all treatment conditions.<sup>39–42</sup>

Concluding the physicochemical analysis of the annealed catalysts, XPS did not reveal significant changes in the composition of Fe<sub>0.5</sub>NC after the cleaning treatments at 600 or 800 °C. This is in line with our interpretations based on the CO chemisorption data that the catalyst surface was not stoichiometrically modified up to 600 °C, and strongly bound adsorbates are more and more removed from CO adsorption sites. The changes observed by XPS after cleaning at 800 °C,

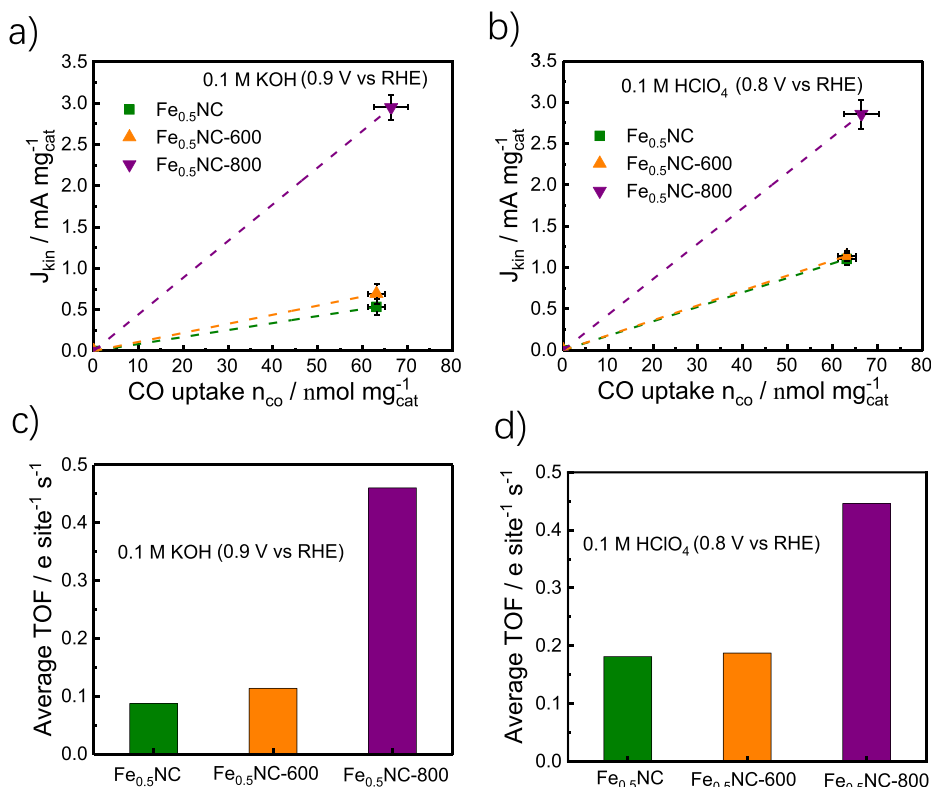


**Figure 6.** Mass-normalized activity, site density and resulting average ORR catalytic TOF values of the Fe<sub>0.5</sub>NC, the Fe<sub>0.5</sub>NC-600, and the Fe<sub>0.5</sub>NC-800 catalysts (see exact values in Tables 2 and 3). Kinetic current density  $J_{kin}$  vs molar CO uptake at (a) 0.9 V<sub>RHE</sub> (alkaline) and (b) at 0.8 V<sub>RHE</sub> (acid). Average TOF values (c) in alkaline and (d) acidic electrolytes.

where markedly higher ORR activity was observed, support the hypothesis that the surface FeN<sub>x</sub> active sites remain present, but their chemical structure or chemical immediate environment was chemically reorganized, likely with respect to the detailed molecular coordination of the central Fe ion in the catalytically active FeN<sub>x</sub> moieties.

**3.3. Evaluation of Active-Site Density (SD) and Turnover Frequency (TOF).** Correlations between the catalyst mass-based voltammetric ORR activity and the corresponding total CO uptake used to evaluate the SD yield information on the intrinsic electrocatalytic activity of probed surface sites of catalysts. In our previously reported CO sorption studies of PGM-free FeNC ORR catalysts, the thermal cleaning temperature had been fixed at 600 °C, driven more by chemical intuition than by understanding.<sup>9,20</sup> The present study demonstrates that 600 °C may indeed be a suitable annealing and cleaning temperature to evaluate SD numbers of PGM-free FeNC ORR electrocatalysts. The temperature is sufficiently high to reach a complete desorption of blocking adsorbates on FeN<sub>x</sub> sites, yet is still sufficiently low to keep thermally induced irreversible chemical transformations of the active sites to a minimum.

The intrinsic catalytic TOF values of the reference Fe<sub>0.5</sub>NC, the Fe<sub>0.5</sub>NC-600, and the Fe<sub>0.5</sub>NC-800 catalysts were derived from the basic relation between TOF, the catalyst mass-normalized voltammetric ORR activity,  $J_{kin}$  and the catalyst mass-normalized FeN<sub>x</sub> SD, given as

$$J_{kin} [\text{A g}^{-1}] = e [\text{C electron}^{-1}] \times \text{TOF} [\text{electron site}^{-1} \text{s}^{-1}] \times \text{SD} [\text{site g}^{-1}] \quad (1)$$

where the mass-based SD is obtained from the experimental molar CO uptake according to

$$\text{SD} [\text{site g}^{-1}] = n_{CO} [\text{nmol mg}^{-1}] \times 10^{-6} \times 6.02310^{23} [\text{site mol}^{-1}] \quad (2)$$

$J_{kin}$  denotes the catalyst mass-based kinetic current at a constant applied working electrode potential (0.8 V<sub>RHE</sub> and 0.9 V<sub>RHE</sub> for acidic and alkaline conditions, respectively, see Table 1),  $e$  is the elementary electron charge, TOF is the turnover frequency in units of electrons transferred per site and per second, and SD the mass-normalized density of accessible active sites on the surface. In eq 2, it is assumed that one molecule CO adsorbs per single FeN<sub>x</sub> site on the surface. Even though FeN<sub>x</sub> sites that are located inside micro pores and may be sterically accessible from two sides might adsorb two CO molecules per site, an overwhelming body of experimental work on a metal porphyrin-metal organic frameworks has shown that the formation of dicarbonyl adducts occurred, if at all, at extremely low temperature (8–80 K), while a mono carbonyl adduct forms preferentially at temperatures above 150 K.<sup>43</sup> Since CO adsorption is performed in the present study at –80 °C (193 K), we can safely assume that only mono carbonyl adducts will form, even for sites that can sterically allow dicarbonyl adducts. This is also supported from recent DFT calculations on a FeN<sub>4</sub>C<sub>10</sub> double-vacancy in graphene, resulting in a stronger binding energy for one molecule of CO adsorbed on FeN<sub>4</sub> than for two CO molecules, –2.64 and –1.42 eV, respectively.<sup>44</sup>

The value of the catalytic ORR activity,  $J_{kin}$  was obtained from a Koutecky–Levich analysis (see Supporting Information) and then normalized by the catalyst mass on the disk

**Table 2.** TOF Data of Fe<sub>0.5</sub>NC, and Fe<sub>0.5</sub>NC-T Catalysts, with T Being the Thermal Pretreatment Temperature in °C

catalyst	TOF in 0.1 M KOH @ 0.9 V <sub>RHE</sub> (e/(site s))	TOF in 0.1 M HClO <sub>4</sub> @ 0.8 V <sub>RHE</sub> (e/(site s))
Fe <sub>0.5</sub> NC	0.09	0.18
Fe <sub>0.5</sub> NC-600	0.12	0.18
Fe <sub>0.5</sub> NC-800	0.46	0.45

electrode. Geometric-area-based current densities and catalyst mass-based activities of the three catalysts in acid and alkaline conditions are listed in Table 1. Their correlation with the CO uptake and the resulting TOF and SD values are reported in Figure 6 and are tabulated in Tables 2 and 3. Note that these values represent averages over all CO-accessible adsorption sites and that they implicitly ascribe the entire experimental ORR activity to CO-adsorbing FeN<sub>x</sub> moieties, which is justified given the negligible catalytic ORR currents at 0.8 V<sub>RHE</sub> and 0.9 V<sub>RHE</sub> on Fe-free N–C catalysts. The ratio between  $J_{\text{kin}}$  and CO uptake is reflected by the slopes of the dashed lines in Figure 5a,b and confirmed that the FeN<sub>x</sub>-sites of the Fe<sub>0.5</sub>NC-800 catalyst displayed a 2×–4× higher TOF, while the TOF values of the reference Fe<sub>0.5</sub>NC and the Fe<sub>0.5</sub>NC-600 catalysts were similar. Using the CO adsorption site nomenclature above, we conclude that multiple thermal cleaning up to 600 °C preserved the chemical nature of the type 1 surface adsorption sites, while the treatment up to 800 °C caused the transformation of type 1 sites into catalytically more active type 2 sites. These findings imply also that multiple or prolonged thermal annealing at 800 °C can be a facile strategy to increase the catalytic TOF of a non PGM catalyst at constant SD value, resulting in an increased catalytic ORR activity. While our physicochemical analysis presented here does not allow for an exhaustive analysis of the surface chemical modifications, it is most likely that the 800 °C cleaning changed the coordinative environment and chemical state of the active FeN<sub>x</sub> sites.

Our findings further suggest that 600 °C is a suitable cleaning temperature to assess the number of surface CO adsorption sites, the site density, the voltammetric ORR activity, and the TOF values accurately. Lower cleaning temperatures result in an underestimation of the relevant site density, as shown in Table 3. Higher cleaning temperatures result in an overestimation of the catalytic TOF, as demonstrated in Table 2.

Finally, we want to compare the present SD values of the Fe<sub>0.5</sub>NC-600 ORR catalysts of Table 3 with previously published values of similar non-PGM catalysts (see Tables

**Table 3.** Site Density (SD) Data Evaluated from CO Sorption Data of the Fe<sub>0.5</sub>NC Reference and All Fe<sub>0.5</sub>NC-T Catalysts

catalyst	CO uptake (nmol/mg <sub>catalyst</sub> )	SD (10 <sup>19</sup> site/g <sub>catalyst</sub> )
Fe <sub>0.5</sub> NC <sup>a</sup>	63.7 ± 2.34	3.84 ± 0.14
Fe <sub>0.5</sub> NC-300	45.15 ± 3.05	2.72 ± 0.26
Fe <sub>0.5</sub> NC-400	50.8 ± 4.8	3.05 ± 0.41
Fe <sub>0.5</sub> NC-500	52.97 ± 1.32	3.19 ± 0.14
Fe <sub>0.5</sub> NC-600	63.14 ± 1.99	3.80 ± 0.21
Fe <sub>0.5</sub> NC-700	63.6 ± 6.23	3.83 ± 0.65
Fe <sub>0.5</sub> NC-800	66.2 ± 3.84	3.99 ± 0.33

<sup>a</sup>The reference Fe<sub>0.5</sub>NC underwent a “standard” thermal cleaning consisting of a single annealing step to 600°C.<sup>9,20</sup> Without thermal pretreatment, CO uptake and SD were zero within the experimental error.

S3 and S4):<sup>9,20</sup> The experimentally determined SD value of 3.8 × 10<sup>19</sup>–3.9 × 10<sup>19</sup> sites per gram of catalyst was in very good agreement with values from FeNC catalysts prepared using a number of different synthesis methods and pathways. PANI-derived Fe<sub>6</sub>NC<sup>9</sup> with a Fe content of 6 wt % exhibited a somewhat higher TOF of 9.1 × 10<sup>19</sup> sites per gram of catalyst, while FeNC catalysts with comparable Fe wt % to Fe<sub>0.5</sub>NC prepared with a secondary N precursor<sup>20</sup> displayed SD values ranging from 3–7 × 10<sup>19</sup> sites per gram of catalyst.

#### 4. CONCLUSIONS

The number of catalytically active sites of a catalyst (i.e., its site density, SD, and the catalytic TOF) are fundamental parameters for a meaningful comparison of the intrinsic reactivity of catalytic materials. They allow a their rational, knowledge-based catalyst development and improvement. SD and TOF values have remained notoriously elusive for PGM-free, metal/nitrogen doped porous carbon electrocatalysts (MNCs), in particular FeNC catalysts, today widely utilized to catalyze the oxygen reduction reaction (ORR) in PGM-free fuel cell cathodes. CO cryo sorption and desorption, with all its shortcomings as ex situ techniques, was demonstrated as a suitable and robust strategy to evaluate SD and TOF numbers of PGM-free electrocatalysts. An integral part of the CO cryo technique was an empirical choice of a thermal pretreatment protocol in order to free up metal sites for CO chemisorption and desorption. The suitability and validity of the previously applied thermal protocol, however, has never been investigated or verified.

This is why we have examined the impact of the cleaning temperature prior to CO-pulse chemisorption on the resulting CO uptake, CO desorption, the SD number, and the TOF numbers during the ORR process using a well-known Fe<sub>0.5</sub>NC catalyst with atomically dispersed FeN<sub>x</sub> moieties. We have revealed that the correct choice of the cleaning temperature is key to obtain accurate SD and TOF values. Detectable CO uptake emerged at 300 °C, as FeN<sub>x</sub> sites were thermally freed up for CO sorption. CO uptake leveled out at 600 °C, resulting in reproducible and physically meaningful SD values of (3–4) × 10<sup>19</sup> site g<sup>-1</sup><sub>catalyst</sub>. These quantitative SD number are in excellent agreement to those of FeNC catalyst prepared by other synthesis methods. Beyond 600 °C cleaning, the catalysts and their active sites underwent a thermally induced chemical transformation into another type of FeN<sub>x</sub> site (here denoted type 2) with enhanced intrinsic catalytic activity. On the basis of our data, in order to ensure accurate SD values derived from CO cryo sorption, we recommend 600 °C as the optimal cleaning temperature for FeNC catalysts.

#### ■ ASSOCIATED CONTENT

##### Supporting Information

The Supporting Information is available free of charge on the ACS Publications website at DOI: 10.1021/acscatal.9b00588.

Additional CO adsorption and TPD data, supporting electrochemical characterization, and TOF data (PDF)

## AUTHOR INFORMATION

## Corresponding Authors

\*E-mail: pstrasser@tu-berlin.de.

\*E-mail: frederic.jaouen@umontpellier.fr.

## ORCID

Chang Hyuck Choi: 0000-0002-2231-6116

Shuang Li: 0000-0001-7414-630X

Arne Thomas: 0000-0002-2130-4930

Frédéric Jaouen: 0000-0001-9836-3261

Peter Strasser: 0000-0002-3884-436X

## Notes

The authors declare no competing financial interest.

## ACKNOWLEDGMENTS

The author would like to acknowledge Dr. Sören Dresch and Dr. Tobias Reier for assistance with RRDE and CO pulse chemisorption experiments. This project received partial financial support by the Graduate School of Excellence Energy Science and Engineering (GRC1070). F.L. acknowledges support by the Berlin International Graduate School for Nature Sciences and Engineering, as well as a China Scholarship Council for the financial support. The research leading to some of these results has received funding from the Fuel Cells and Hydrogen 2 Joint Undertaking under grant agreement no. 779366. This Joint Undertaking receives support from the European Union's Horizon 2020 research and innovation program, Hydrogen Europe and Hydrogen Europe research. C.H.C. acknowledges the support by Creative Materials Discovery Program through the National Research Foundation of Korea (NRF) funded by Ministry of Science and ICT (NRF-2017M3D1A1039378).

## REFERENCES

(1) Wu, G.; More, K. L.; Johnston, C. M.; Zelenay, P. High-Performance Electrocatalysts for Oxygen Reduction Derived from Polyaniline, Iron, and Cobalt. *Science* **2011**, *332* (6028), 443–447.

(2) Proietti, E.; Jaouen, F.; Lefevre, M.; Larouche, N.; Tian, J.; Herranz, J.; Dodelet, J. P. Iron-based cathode catalyst with enhanced power density in polymer electrolyte membrane fuel cells. *Nat. Commun.* **2011**, *2*, 416.

(3) Chen, Z.; Higgins, D.; Yu, A.; Zhang, L.; Zhang, J. Aiping Yu, Lei Zhang, Jiujun Zhang, A review on non-precious metal electrocatalysts for PEM fuel cells. *Energy Environ. Sci.* **2011**, *4*, 3167–3192.

(4) Wang, Z. L.; Xu, D.; Xu, J. J.; Zhang, X. B. Oxygen electrocatalysts in metal-air batteries: from aqueous to nonaqueous electrolytes. *Chem. Soc. Rev.* **2014**, *43* (22), 7746–86.

(5) Spalek, O. Oxygen trickle-bed electrode as a cathode for chlor-alkali electrolysis. *J. Appl. Electrochem.* **1994**, *24*, 751–757.

(6) Li, J.; Jia, Q.; Ghoshal, S.; Liang, W.; Mukerjee, S. Highly Active and Stable Fe-N-C Catalyst for Oxygen Depolarized Cathode Applications. *Langmuir* **2017**, *33* (37), 9246–9253.

(7) Lefevre, M.; Proietti, E.; Jaouen, F.; Dodelet, J.-P. Iron-Based Catalysts with Improved Oxygen Reduction Activity in Polymer Electrolyte Fuel Cells. *Science* **2009**, *324*, 71–74.

(8) Jaouen, F.; Proietti, E.; Lefevre, M.; Chenitz, R.; Dodelet, J.-P.; Wu, G.; Chung, H. T.; Johnston, C. M.; Zelenay, P. Recent advances in non-precious metal catalysis for oxygen-reduction reaction in polymer electrolyte fuelcells. *Energy Environ. Sci.* **2011**, *4* (1), 114–130.

(9) Sahraie, N. R.; Kramm, U. I.; Steinberg, J.; Zhang, Y.; Thomas, A.; Reier, T.; Paraknowitsch, J. P.; Strasser, P. Quantifying the density and utilization of active sites in non-precious metal oxygen electroreduction catalysts. *Nat. Commun.* **2015**, *6*, 8618.

(10) Malko, D.; Kucernak, A.; Lopes, T. In situ electrochemical quantification of active sites in Fe-N/C non-precious metal catalysts. *Nat. Commun.* **2016**, *7*, 13285.

(11) Kneebone, J. L.; Daifuku, S. L.; Kehl, J. A.; Wu, G.; Chung, H. T.; Hu, M. Y.; Alp, E. E.; More, K. L.; Zelenay, P.; Holby, E. F.; Neidig, M. L. A Combined Probe-Molecule, Mössbauer, Nuclear Resonance Vibrational Spectroscopy, and Density Functional Theory Approach for Evaluation of Potential Iron Active Sites in an Oxygen Reduction Reaction Catalyst. *J. Phys. Chem. C* **2017**, *121* (30), 16283–16290.

(12) Chen, Y.; Artyushkova, K.; Rojas-Carbonell, S.; Serov, A.; Matanovic, I.; Santoro, C.; Asset, T.; Atanassov, P. Inhibition of Surface Chemical Moieties by Tris(hydroxymethyl)aminomethane: A Key to Understanding Oxygen Reduction on Iron-Nitrogen-Carbon Catalysts. *ACS Applied Energy Materials*. **2018**, *1* (5), 1942–1949.

(13) Thorum, M. S.; Hankett, J. M.; Gewirth, A. A. Poisoning the Oxygen Reduction Reaction on Carbon-Supported Fe and Cu Electrocatalysts: Evidence for Metal-Centered Activity. *J. Phys. Chem. Lett.* **2011**, *2* (4), 295–298.

(14) Chung, M. W.; Chon, G.; Kim, H.; Jaouen, F.; Choi, C. H. Electrochemical Evidence for Two Sub-families of Fe<sub>N</sub>xC<sub>y</sub> Moieties with Concentration-Dependent Cyanide Poisoning. *ChemElectroChem* **2018**, *5* (14), 1880–1885.

(15) Chakraborty, A.; Devivaraprasad, R.; Bera, B.; Neergat, M. Electrochemical estimation of the active site density on metal-free nitrogen-doped carbon using catechol as an adsorbate. *Phys. Chem. Chem. Phys.* **2017**, *19* (37), 25414–25422.

(16) Birry, L.; Zagal, J. H.; Dodelet, J.-P. Does CO poison Fe-based catalysts for ORR? *Electrochem. Commun.* **2010**, *12* (5), 628–631.

(17) Guo, N.; Fingland, B. R.; Williams, W. D.; Kispersky, V. F.; Jelic, J.; Delgass, W. N.; Ribeiro, F. H.; Meyer, R. J.; Miller, J. T. Determination of CO, H<sub>2</sub>O and H<sub>2</sub> coverage by XANES and EXAFS on Pt and Au during water gas shift reaction. *Phys. Chem. Chem. Phys.* **2010**, *12* (21), 5678–93.

(18) Liu, L.; Zhou, F.; Wang, L.; Qi, X.; Shi, F.; Deng, Y. Low-temperature CO oxidation over supported Pt, Pd catalysts: Particular role of FeO<sub>x</sub> support for oxygen supply during reactions. *J. Catal.* **2010**, *274* (1), 1–10.

(19) Zhang, Q.; Mamtani, K.; Jain, D.; Ozkan, U.; Asthagiri, A. CO Poisoning Effects on FeNC and CN<sub>x</sub> ORR Catalysts: A Combined Experimental-Computational Study. *J. Phys. Chem. C* **2016**, *120* (28), 15173–15184.

(20) Leonard, N. D.; Wagner, S.; Luo, F.; Steinberg, J.; Ju, W.; Weidler, N.; Wang, H.; Kramm, U. I.; Strasser, P. Deconvolution of Utilization, Site Density, and Turnover Frequency of Fe-Nitrogen-Carbon Oxygen Reduction Reaction Catalysts Prepared with Secondary N-Precursors. *ACS Catal.* **2018**, *8* (3), 1640–1647.

(21) Zitolo, A.; Goellner, V.; Armel, V.; Sougrati, M.-T.; Mineva, T.; Stievano, L.; Fonda, E.; Jaouen, F. Identification of catalytic sites for oxygen reduction in iron- and nitrogen-doped graphene materials. *Nat. Mater.* **2015**, *14* (9), 937–942.

(22) Zitolo, A.; Ranjbar-Sahraie, N.; Mineva, T.; Li, J.; Jia, Q.; Stamatina, S.; Harrington, G. F.; Lyth, S. M.; Krtil, P.; Mukerjee, S.; Fonda, E.; Jaouen, F. Identification of catalytic sites in cobalt-nitrogen-carbon materials for the oxygen reduction reaction. *Nat. Commun.* **2017**, *8* (1), 957.

(23) Koslowski, U. I.; Abs-Wurmbach, I.; Fiechter, S.; Bogdanoff, P. Nature of the catalytic centres of porphyrin based electrocatalysts for the ORR—a correlation of kinetic current density with the site density of Fe-N<sub>4</sub> centres. *J. Phys. Chem. C* **2008**, *112*, 15356–15366.

(24) Kramm, U. I.; Herranz, J.; Larouche, N.; Arruda, T. M.; Lefevre, M.; Jaouen, F.; Bogdanoff, P.; Fiechter, S.; Abs-Wurmbach, I.; Mukerjee, S.; Dodelet, J. P. Structure of the catalytic sites in Fe/N/C-catalysts for O<sub>2</sub>-reduction in PEM fuel cells. *Phys. Chem. Chem. Phys.* **2012**, *14* (33), 11673–88.

(25) Serov, A.; Artyushkova, K.; Niangar, E.; Wang, C.; Dale, N.; Jaouen, F.; Sougrati, M.-T.; Jia, Q.; Mukerjee, S.; Atanassov, P. Nano-structured non-platinum catalysts for automotive fuel cell application. *Nano Energy* **2015**, *16*, 293–300.

- (26) Chenitz, R.; Kramm, U. I.; Lefèvre, M.; Glibin, V.; Zhang, G.; Sun, S.; Dodelet, J.-P. A specific demetalation of Fe-N<sub>4</sub> catalytic sites in the micropores of NC/Ar + NH<sub>3</sub> is at the origin of the initial activity loss of the highly active Fe/N/C catalyst used for the reduction of oxygen in PEM fuel cells. *Energy Environ. Sci.* **2018**, *11* (2), 365–382.
- (27) Choi, C. H.; Choi, W. S.; Kasian, O.; Mechler, A. K.; Sougrati, M. T.; Bruller, S.; Strickland, K.; Jia, Q.; Mukerjee, S.; Mayrhofer, K. J. J.; Jaouen, F. Unraveling the Nature of Sites Active toward Hydrogen Peroxide Reduction in Fe-N-C Catalysts. *Angew. Chem.* **2017**, *129*, 8935.
- (28) Ramaswamy, N.; Tylus, U.; Jia, Q.; Mukerjee, S. Activity descriptor identification for oxygen reduction on nonprecious electrocatalysts: linking surface science to coordination chemistry. *J. Am. Chem. Soc.* **2013**, *135* (41), 15443–9.
- (29) Wang, S.; Li, X.; Zhao, Z.; Li, Z. Zhenxia Zhao and Zhong Li, Competitive Adsorption of Carbon Monoxide and Water Vapour on MIL-100(Fe) Prepared Using a Microwave Method. *Adsorpt. Sci. Technol.* **2015**, *33* (3), 279–296.
- (30) Jaouen, F. D. R.; Dodelet, J.-P. O<sub>2</sub> Reduction Mechanism on Non-Noble Metal Catalysts for PEM Fuel Cells. Part I: Experimental Rates of O<sub>2</sub> Electroreduction, H<sub>2</sub>O<sub>2</sub> Electroreduction, and H<sub>2</sub>O<sub>2</sub> Disproportionation. *J. Phys. Chem. C* **2009**, *113* (34), 15422–15432.
- (31) Artyushkova, K.; Kiefer, B.; Halevi, B.; Knop-Gericke, A.; Schlögl, R.; Atanassov, P. Density functional theory calculations of XPS binding energy shift for nitrogen-containing graphene-like structures. *Chem. Commun. (Cambridge, U. K.)* **2013**, *49* (25), 2539–41.
- (32) Artyushkova, K.; Serov, A.; Rojas-Carbonell, S.; Atanassov, P. Chemistry of Multitudinous Active Sites for Oxygen Reduction Reaction in Transition Metal-Nitrogen-Carbon Electrocatalysts. *J. Phys. Chem. C* **2015**, *119* (46), 25917–25928.
- (33) Kattel, S.; Atanassov, P.; Kiefer, B. Density Functional Theory Study of Ni-N<sub>x</sub>/C Electrocatalyst for Oxygen Reduction in Alkaline and Acidic Media. *J. Phys. Chem. C* **2012**, *116* (33), 17378–17383.
- (34) Kattel, S.; Atanassov, P.; Kiefer, B. Catalytic activity of Co-N(x)/C electrocatalysts for oxygen reduction reaction: a density functional theory study. *Phys. Chem. Chem. Phys.* **2013**, *15* (1), 148–53.
- (35) Kattel, S.; Atanassov, P.; Kiefer, B. A density functional theory study of oxygen reduction reaction on non-PGM Fe-N<sub>x</sub>-C electrocatalysts. *Phys. Chem. Chem. Phys.* **2014**, *16* (27), 13800–6.
- (36) Qian, Y.; Du, P.; Wu, P.; Cai, C.; Gervasio, D. F. Chemical Nature of Catalytic Active Sites for the Oxygen Reduction Reaction on Nitrogen-Doped Carbon-Supported Non-Noble Metal Catalysts. *J. Phys. Chem. C* **2016**, *120* (18), 9884–9896.
- (37) Ju, W.; Bagger, A.; Hao, G. P.; Varela, A. S.; Sinev, I.; Bon, V.; Roldan Cuenya, B.; Kaskel, S.; Rossmeisl, J.; Strasser, P. Understanding activity and selectivity of metal-nitrogen-doped carbon catalysts for electrochemical reduction of CO<sub>2</sub>. *Nat. Commun.* **2017**, *8* (1), 944.
- (38) Möller, T.; Ju, W.; Bagger, A.; Wang, X.; Luo, F.; Ngo Thanh, T.; Varela, A. S.; Rossmeisl, J.; Strasser, P. Efficient CO<sub>2</sub> to CO electrolysis on solid Ni-N-C catalysts at industrial current densities. *Energy Environ. Sci.* **2019**, *12* (2), 640–647.
- (39) Choudhury, T.; Saied, S. O.; Sullivan, J. L.; Abbot, A. M. Reduction of oxides of iron, cobalt, titanium and niobium by low-energy ion bombardment. *J. Phys. D: Appl. Phys.* **1989**, *22* (8), 1185.
- (40) Fu, X.; Liu, Y.; Cao, X.; Jin, J.; Liu, Q.; Zhang, J. FeCo-N<sub>x</sub> embedded graphene as high performance catalysts for oxygen reduction reaction. *Appl. Catal., B* **2013**, *130–131*, 143–151.
- (41) Faubert, G.; Côté, R.; Dodelet, J. P.; Lefèvre, M.; Bertrand, P. Oxygen reduction catalysts for polymer electrolyte fuel cells from the pyrolysis of FeII acetate adsorbed on 3,4,9,10-perylenetetracarboxylic dianhydride. *Electrochim. Acta* **1999**, *44* (15), 2589–2603.
- (42) Li, S.; Zhang, L.; Kim, J.; Pan, M.; Shi, Z.; Zhang, J. Synthesis of carbon-supported binary FeCo-N non-noble metal electrocatalysts for the oxygen reduction reaction. *Electrochim. Acta* **2010**, *55* (24), 7346–7353.
- (43) Gallagher, A. T.; Malliakas, C. D.; Harris, T. D. CO Binding at a Four-Coordinate Cobaltous Porphyrin Site in a Metal-Organic Framework: Structural, EPR, and Gas Adsorption Analysis. *Inorg. Chem.* **2017**, *56* (8), 4654–4661.
- (44) Omidvar, A. Charge-controlled switchable CO adsorption on FeN<sub>4</sub> cluster embedded in graphene. *Surf. Sci.* **2018**, *668*, 117–124.